Thermoforming Plastic Cups and Cones

by

MELISSA ANN KERSHNER

A thesis submitted in partial fulfillment of the requirement for the degree of

MASTER OF SCIENCE
in Mechanical Engineering

at the

UNIVERSITY OF WISCONSIN-MADISON

2007

Approved

_____

A. Jeffrey Giacomin

Professor of Mechanical Engineering

Date_____

Table of Contents

ACKNOWLEDGEMENT

I am deeply grateful to my advisor Professor Giacomin, whose knowledge and insight I could not have finished without. I would especially like to thank him and the other committee members Professor Osswald and Professor Turng for their support and guidance. Also, through their courses I have gained valuable knowledge that I will use for the rest of my career.

Thank you to Dr. Jaydeep Kulkarni of Fluent Corporation for guidance with the Finite Element software. I am also indebted to the Fluent Corporation for generously extending an academic license to the Rheology Research Center of the University of Wisconsin for the POLYFLOW finite element simulation software.

Also, I am grateful to Dr. Zhongbao Chen of the University of Wisconsin and Dr. Martin Stephenson for their technical advice. I also wish to acknowledge Professor R. Byron Bird of the University of Wisconsin for his help with the thin film approximation.

I would also like to extend a special thanks to the students of the Polymer Engineering Society and in my lab. They have given me very helpful direction during my research. I have thoroughly enjoyed working with them.

Last but not least, thank you to all the members of the Industrial Consortium of the Center for Advanced Polymer for financial support, especially the Placon Corporation of Madison, Wisconsin and Plastics Ingenuity Inc. of Cross Plains, Wisconsin.

DEDICATION

To my family and future husband Andrew Ju for all their love and support.

List of Figures

Part I: Thermoforming Cones

Part II: Thermoforming Cups

Part I: Thermoforming Cones

Abstract

This new analysis for thermoforming cones focuses on the manufacturing process speed. Specifically, this work distinguishes between what happens before and after (free versus constrained forming) the melt touches the conical mold. Analytical solutions are derived for the time required for both cases, and sum them to get the total forming time. This analysis is restricted to the Newtonian fabrication of cones, the simplest relevant problem in commercial thermoforming.

I. Introduction

Thermoforming is the mass production of thin non-hollow products from uniformly thick flat sheets. We divide modern commercial thermoforming into four phases. Firstly, in **free forming** (ϕ), a thin untouched sheet deforms under an applied air pressure. In **plug assisted forming** (π), a carefully designed solid shape then touches and stretches some of the sheet to reshape it. The parts touching the plug do not stretch. Once released from this plug, the reshaped sheet again deforms freely till it contacts the mold. The material not yet touching the mold then continues to stretch till the mold is covered and we call this **constrained forming** (κ). Sometimes, thermoforming is done without the plug assist and this paper attacks this special case. Tadmor and Gogos [1] call this **straight thermoforming**. We solve for both the mold covering speed and the product thickness profile. Table 1 compares this paper with previous work.

We begin by modeling free forming, where a uniformly thin polymeric film is formed from a thin flat disk inflated through a round hole into a growing thin sphere. Williams [4] confirmed this spherical shape experimentally. These thin spheres transition from lenticular, through hemispherical, to bulbous as illustrated in Figure 1. Figure 2 illustrates the initial condition, a flat disk of thickness h_0, and thus of infinite radius of curvature, R.

We restrict this analysis to Newtonian liquids, so we expect this work will apply accurately to low molecular weight systems such as polyester which is commonly used to thermoform stiff clear packaging. Our analytical solutions also provide benchmarks for numerical analysts to test their code accuracy. We further restrict our analysis to the fabrication of cones, the simplest product shape in commercial thermoforming.

Table 2 summarizes these and other dimensional variables. Furthermore, Table 3 defines the corresponding dimensionless variables, including thickness (T), radius of curvature (ρ) and height (H) of the free forming bubble.

	Cylinder	Cone	Truncated Cone	Wedge	Truncated Wedge	Phases	Tensile Stresses	Geometry	Constitutive Behavior	Uniform Thickness	Speed	Reference
Hart-Smith and Crisp (1967)						ϕ	**X**	**X**	σ			[2]
Sheryshev et al. (1969)	**X**					κ		**X**		**X**		[3]
Williams (1970)	**X**	**X**				ϕ, π	**X**	**X**	σ	**X**		[4]
Williams (1970)				**X**	**X**	κ, π	**X**	**X**	σ			[4]
Tadmor and Gogos (1979)		**X**				κ		**X**		**X**		[1]
Rosenzweig et al. (1979)		**X**	**X**			κ		**X**		**X**		[5]
Throne (1979)	**X**					κ, π		**X**	σ	**X**		[6]
Pearson (1985)	**X**	**X**		**X**		κ	**X**	**X**	σ	**X**		[7]
Allard et al. (1986)	**X**		**X**			ϕ, κ	**X**	**X**	λ	**X**		[8]
Baird and Collias (1998)		**X**				κ		**X**	λ	**X**		[9]
Osswald and Hernández – Ortiz (2006)		**X**				κ		**X**		**X**		[10]
This Paper		**X**	**X**			ϕ, π, κ	**X**	**X**	λ	**X**	**X**	

Table 1: Previous work [free forming (ϕ), plug assisted forming (π), constrained forming (κ); liquid (λ), solid (σ)]

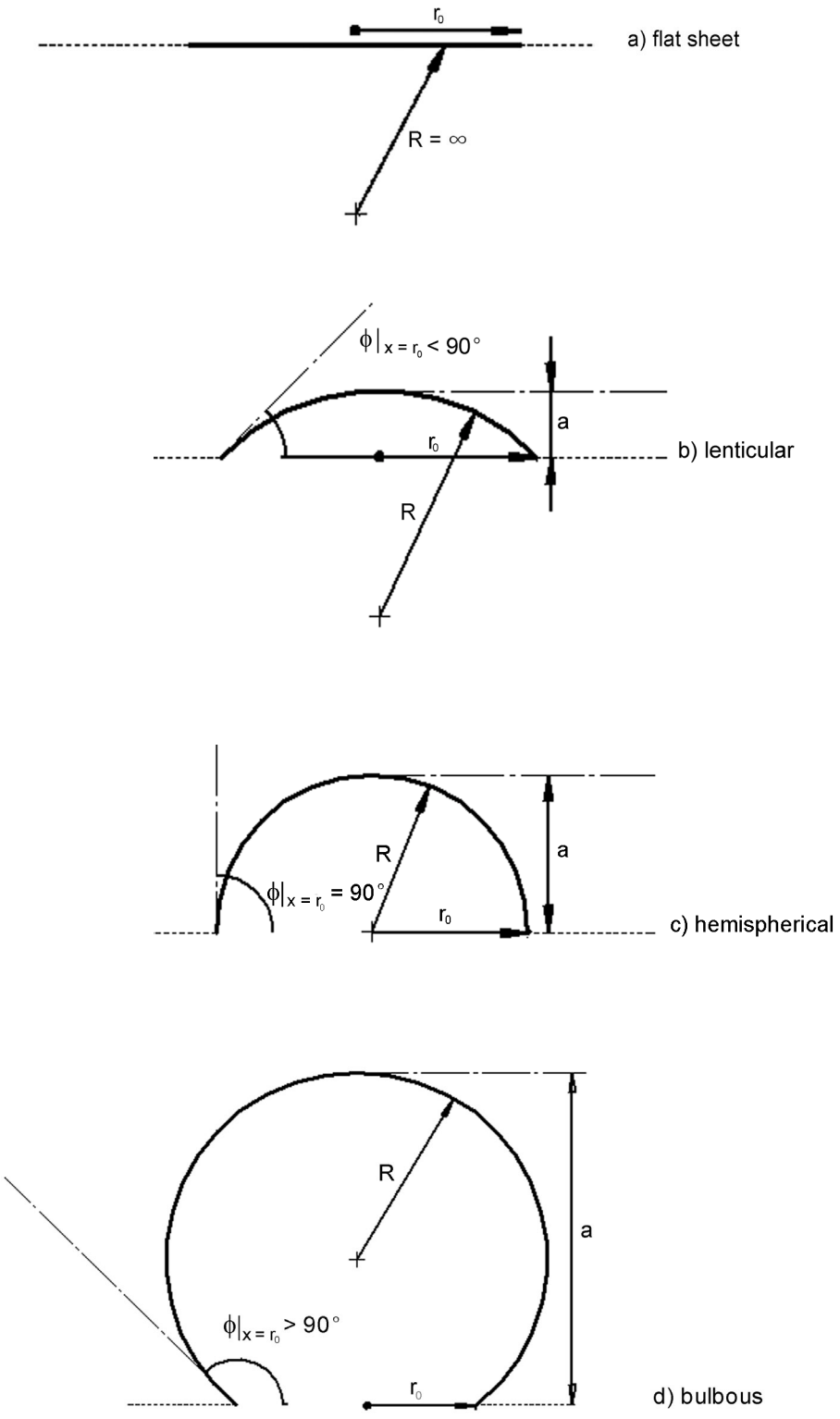

Figure 1 : Thin sphere transitioning

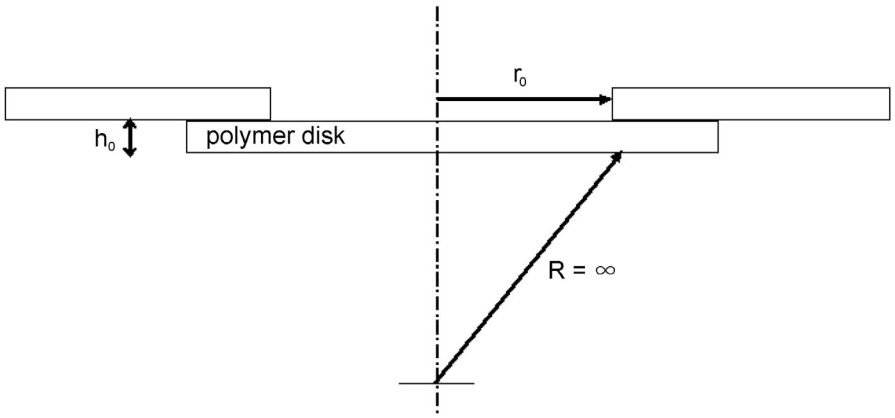

Figure 2: Initial undeformed disk (just before thermoforming).

Name	Symbol
Initial disk thickness	h_0
Bubble height	a
Radius of curvature	R
Slit radius	$r_0 \equiv \frac{L}{\tan\beta}$
Time	t
Final thickness	h
Contact angle of sheet's edge	ϕ
Contact length	z_k
Pressure drop	$\Delta P \equiv P_i - P_o$
Inner pressure	P_i
Outer pressure	P_o
Plug radius	R_π
Plug displacement	d_π
Cone apex sharpness	R_f
Finished part height	H_p
Free forming interval	t_ϕ
Constrained forming interval	t_κ
Thickness during constrained forming	h_κ

Table 2: Dimensional variables

Name	Symbol	Definition
Thickness	T	h/h_0
Radius of curvature	ρ	R/r_0
Bubble height	H	a/r_0
Free forming time	θ	$\frac{\Delta P t}{12\mu}$
Constrained forming time	Θ	$\frac{\Delta P t}{12\mu}$
Free forming interval	θ_ϕ	$\left.\frac{\Delta P t}{12\mu}\right\|_{\rho=\rho_\kappa}$
Constrained forming interval	Θ_κ	$\left.\frac{\Delta P t}{12\mu}\right\|_{\rho=\rho_f}$
Total forming time	Π	$\theta_\phi + \Theta_\kappa$
Draw ratio [11]	ℓ	$\frac{L}{2r_0} = \frac{tan\,\beta}{2}$
Cone height		2ℓ
Conical melt length	Z_κ	z_k/r_0
Thickness during constrained forming	T_κ	h/h_κ
Melt radius of curvature when constrained forming begins	ρ_κ	R_κ/r_0
Sheet uniformity	Υ	$\frac{h(z_{\kappa f})}{h(z_\kappa=0)}$
Cone shape factor	α	$\frac{1+\cos\beta}{2\alpha_0}\left(\frac{\sin^2\beta}{2\ell\cos\beta}\right)^{1-\sec\beta}$
Stress	Σ_{ij}	$\frac{\tau_{ij}}{\Delta P}$
Disk shape	α_0	h_0/r_0
Plug shape factor	α_π	R_π/r_0
Cone apex sharpness	ρ_f	R_f/r_0
Centerline proximity	ω	r/r_0
Stroke	σ	d_π/L

Table 3: Dimensionless variables and groups

II. Thermoforming Mechanics

For the mechanics of the stretching sheet, we follow the thin membrane approach for bubble inflation of Baird and Collias [9]. We employ moving spherical coordinates centered in the bubble. Figure 1 defines *r*. Assuming constant density, the continuity equation becomes

$$\frac{\partial}{\partial r}\left(r^2 v_r\right) = 0 \tag{1}$$

Integrating gives:

$$v_r = \frac{A(t)}{r^2} \tag{2}$$

where $A(t)$ is a function of time. On the inside surface (at $r = R$) the fluid velocity is

$$v_r(R) = -\dot{R} \tag{3}$$

for a lenticular film, and for a bulbous one:

$$v_r(R) = \dot{R} \tag{4}$$

hence

$$A(t) = \left|\dot{R}\right| R^2 \tag{5}$$

and from continuity

$$v_r = \frac{\left|\dot{R}\right| R^2}{r^2} \tag{6}$$

Neglecting fluid inertia, the *r*-component of the equation of motion reduces to

$$0 = \frac{-\partial p}{\partial r} - \frac{1}{r^2}\frac{\partial}{\partial r}\left(r^2 \tau_{rr}\right) + \frac{\tau_{\theta\theta} + \tau_{\phi\phi}}{r} \tag{7}$$

where τ_{ij} is the component of the extra stress tensor corresponding to the flux of x_j momentum in the positive x_i direction. Hence, $\tau_{\phi\phi}$ and $\tau_{\theta\theta}$ are negative in tension. Rewriting (7):

$$\frac{\partial \pi_{rr}}{\partial r} = \frac{\tau_{\theta\theta} + \tau_{\phi\phi} - 2\tau_{rr}}{r} \tag{8}$$

where the *rr* component of the total and extra stress tensors are related by

$$\pi_{rr} = \tau_{rr} + p \tag{9}$$

where at the inside surface

$$\pi_{rr}(R) = -P(R) \tag{10}$$

and outside,

$$\pi_{rr}(R+h) = -P(R+h) \tag{11}$$

Integrating, the equation of motion [(7)] gives

$$\Delta P = \int_R^{R+h} \left[\frac{\tau_{\theta\theta} + \tau_{\phi\phi} - 2\tau_{rr}}{r} \right] dr \tag{12}$$

For thin films, that is, when:

$$\frac{h}{h_0} << 1 \tag{13}$$

Bird *et al.* [12] proposed that the argument for the integral in (12), $\left(\tau_{\theta\theta} + \tau_{\phi\phi} - 2\tau_{rr}\right)/r$ will be nearly constant. This is because, for a thin film, neither the stresses $\left(\tau_{\theta\theta} + \tau_{\phi\phi} - 2\tau_{rr}\right)$, nor the radial position r, will vary much through the film thickness. Thus, (12) becomes:

$$\Delta P = \left(\tau_{\theta\theta} + \tau_{\phi\phi} - 2\tau_{rr}\right)\frac{h}{R} \tag{14}$$

We call this the *thin film approximation*, and Appendix A further explores its importance.

We can thus further simplify (14), by specifically evaluating the stresses at $r = R$:

$$\Delta P = \left(\tau_{\theta\theta} + \tau_{\phi\phi} - 2\tau_{rr}\right)\Big|_R \frac{h}{R} \tag{15}$$

For a Newtonian fluid:

$$\tau_{\theta\theta} = \tau_{\phi\phi} = -2\mu\frac{v_r}{r} = \frac{-2\mu R^2\left|\dot{R}\right|}{r^3} \tag{16}$$

and

$$\tau_{rr} = -2\mu\frac{\partial v_r}{\partial r} = \frac{4\mu R^2\left|\dot{R}\right|}{r^3} \tag{17}$$

Thus the tensile stress inside the stretching film:

$$\tau_{\theta\theta}{}^{i} = \frac{-\tau_{rr}{}^{i}}{2} = \frac{-2\mu R^2\left|\dot{R}\right|}{R^3} \tag{18}$$

exceeds the stress outside:

$$\tau_{\theta\theta}{}^{o} = \frac{-\tau_{rr}{}^{o}}{2} = \frac{-2\mu R^2\left|\dot{R}\right|}{\left(R+h\right)^3} \tag{19}$$

by the factor:

$$\frac{\tau_{\theta\theta}{}^{o}}{\tau_{\theta\theta}{}^{i}} = \frac{\tau_{rr}{}^{o}}{\tau_{rr}{}^{i}} = \left(1+\frac{h}{R}\right)^3 \tag{20}$$

Eliminating the stresses in (15) gives

$$\Delta P = \frac{12\mu\left|\dot{R}\right|h}{R^2} \tag{21}$$

which reduces to

$$\frac{\Delta P\rho^2}{12\mu T\alpha_0} = \left|\frac{d\rho}{dt}\right| \tag{22}$$

which has been adimensionalized using Table 3. Hence,

$$\left|\frac{d\rho}{d\theta}\right| = \frac{\rho^2}{T\alpha_0} \tag{23}$$

which describes how a thin disk's shape evolves during thermoforming.[1]

III. Free Forming Geometry

The lenticular spherical cap thickness depends on its radius of curvature as

$$T = \frac{\rho + \left|\sqrt{\rho^2 - 1}\right|}{2\rho}; T \geq \frac{1}{2} \tag{24}$$

so that

$$\frac{dT}{d\rho} = \frac{1}{2\rho\left|\sqrt{\rho^2 - 1}\right|}; T > \frac{1}{2} \tag{25}$$

and for the bulbous spherical cap

$$T = \frac{\rho - \left|\sqrt{\rho^2 - 1}\right|}{2\rho}; T \leq \frac{1}{2} \tag{26}$$

so that

$$\frac{dT}{d\rho} = \frac{-1}{2\rho\left|\sqrt{\rho^2 - 1}\right|}; T < \frac{1}{2} \tag{27}$$

The following discontinuity thus occurs

$$\left.\frac{dT}{d\rho}\right|_{T \to \frac{1}{2}^{\pm}} = \pm\frac{1}{4} \tag{28}$$

We obtain the *contact angle of the sheet's edge* (defined in Figure 1) from the bubble's slope evaluated at r_0:

[1] By definition, the dimensionless radius of curvature, ρ, never falls below unity.

$$\phi|_{x=r_0} = \frac{\pi}{2} + a\tan\frac{-1}{\left|\sqrt{\rho^2-1}\right|} \tag{29}$$

With difficulty, practitioners can sometimes observe the free forming bubble and measure its height (defined as a in Figure 1). The dimensionless bubble height depends on its radius of curvature for the lenticular shape as

$$H = \rho - \left|\sqrt{\rho^2-1}\right|; H \geq 1 \tag{30}$$

and for the bulbous shape

$$H = \rho + \left|\sqrt{\rho^2-1}\right|; H \leq 1 \tag{31}$$

IV. Free Forming Results

Substituting (22) into (21) for T, for a lenticular cap we get

$$\left|\frac{d\rho}{d\theta}\right| = \frac{2\rho^3}{\alpha_0\left(\rho + \left|\sqrt{\rho^2-1}\right|\right)} \tag{32}$$

Integrating gives

$$\theta = \frac{\alpha_0}{4}\left[-arcsin\left(\frac{1}{\rho}\right) - \sqrt{\frac{\rho^2-1}{\rho^4}} + \frac{2}{\rho}\right] \tag{33}$$

for bulbous cap growth, and for lenticular cap growth, we substitute (24) into (21)for T, and integrate

$$\left|\frac{d\rho}{d\theta}\right| = \frac{2\rho^3}{\alpha_0\left(\rho - \left|\sqrt{\rho^2-1}\right|\right)} \tag{34}$$

to get

$$\theta = \frac{\alpha_0}{4}\left[arcsin\left(\frac{1}{\rho}\right) + \sqrt{\frac{\rho^2 - 1}{\rho^4}} - \frac{2}{\rho} - \pi + 4 \right] \tag{35}$$

Eqs. (33) and (35) are universal, and central to this paper. From these we see that the shape switch from lenticular to bulbous always occurs at the same dimensionless time when,

$$\theta|_{\rho=1} > \frac{\alpha_0}{8}(4 - \pi) \tag{36}$$

where.

$$\left.\frac{d\rho}{d\theta}\right|_{\rho=1} = 0 \tag{37}$$

Figure 3 illustrates this shape switch.

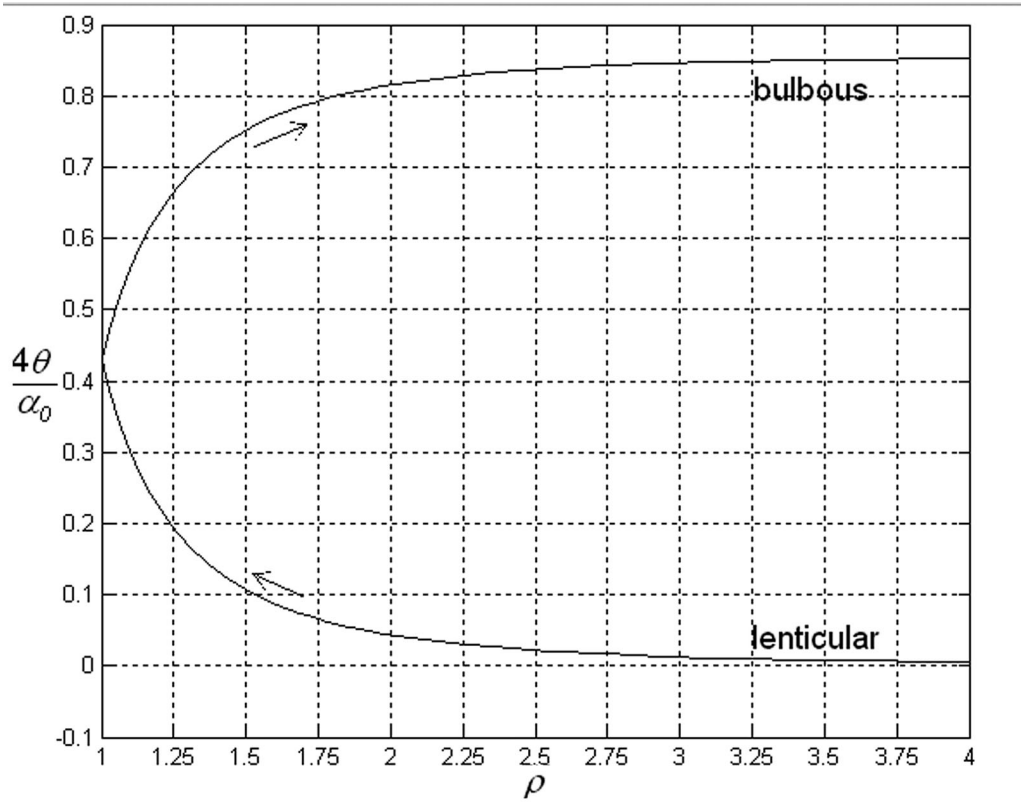

Figure 3: Dimensionless radius of curvature as a function of dimensionless time.

Adimensionalizing (18) gives the dimensionless hoop stress inside the stretching film:

$$\Sigma_{\phi\phi} = \frac{-1}{6\rho}\left|\frac{d\rho}{d\theta}\right| \tag{38}$$

For the lenticular melt,

$$\alpha_0\Sigma_{\phi\phi} = \frac{-\rho^2}{3\left(\rho + \left|\sqrt{\rho^2 - 1}\right|\right)} \tag{39}$$

which is negative and peaks at

$$\rho = \frac{2}{\sqrt{3}} \tag{40}$$

where

$$\alpha_0\Sigma_{\phi\phi} = \frac{-4\sqrt{3}}{27} \cong -0.257 \tag{41}$$

and for the bulbous melt

$$\alpha_0\Sigma_{\phi\phi} = \frac{-\rho^2}{3\left(\rho - \left|\sqrt{\rho^2 - 1}\right|\right)} \tag{42}$$

Figure 4 illustrates this. So both the radius of curvature and the magnitude of the tensile stress, $\left|\Sigma_{\phi\phi}\right|$, are initially infinite. In practice, there is always a little sag [13, 14], so the initial radius of curvature is always finite. Furthermore, unlike a rubber, $\left|\Sigma_{\phi\phi}\right|$ is initially increasing.

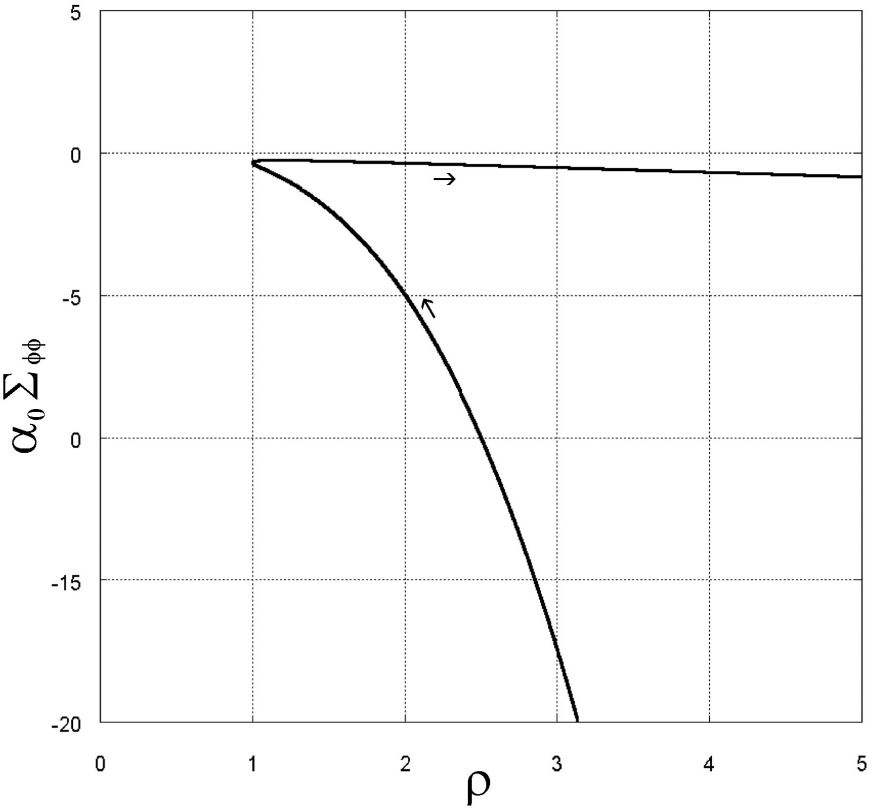

Figure 4: Dimensionless stress versus dimensionless radius of curvature.

V. Constrained Forming Geometry

The constrained melt takes on the shape of the conical mold, as shown in Figure 5. A lenticular melt forms into a lenticular cone, and a bulbous melt forms into a bulbous cone.

From geometry and the mass balance we can relate the dimensionless radius of curvature to the conical melt length [9]

$$\rho = \frac{2\ell - Z_\kappa \sin\beta}{\sin\beta \tan\beta} \tag{43}$$

Now free-forming ends when melt first touches the cone, that is, when $Z_k = 0$. Hence,

$$\rho_\kappa = \frac{2\ell}{\sin\beta\tan\beta} \tag{44}$$

Substituting into (33) and (35) gives the free-forming intervals, θ_ϕ, for the bulbous melt:

$$\theta_\phi = \frac{\alpha_0}{4}\left[-arcsin\left(\frac{1}{\rho_\kappa}\right) - \frac{\sqrt{\rho_\kappa{}^2 - 1}}{\rho_\kappa{}^4} + \frac{2}{\rho_\kappa}\right] \tag{45}$$

and for the lenticular melt:

$$\theta_\phi = \frac{\alpha_0}{4}\left[arcsin\left(\frac{1}{\rho_\kappa}\right) + \frac{\sqrt{\rho_\kappa{}^2 - 1}}{\rho_\kappa{}^4} - \frac{2}{\rho_\kappa} - \pi + 4\right] \tag{46}$$

respectively. We can also relate the constrained melt thickness t, to the contact length [1]

$$T = T_\kappa\left(1 - \frac{Z_\kappa}{2\ell}sin\beta\right)^{sec\beta - 1} \tag{47}$$

From geometry, we can relate the thickness during constrained forming, h_κ to the initial disk thickness

$$\frac{\pi L^2 h_0}{4} = \frac{\pi L^2(1 - cos\beta)h_\kappa}{2sin^2\beta} \tag{48}$$

which adimensionalizes to

$$T_\kappa = \frac{T_0}{2}(1 + cos\beta) \tag{49}$$

or

$$T_\kappa = \frac{1}{2}(1 + cos\beta) \tag{50}$$

.

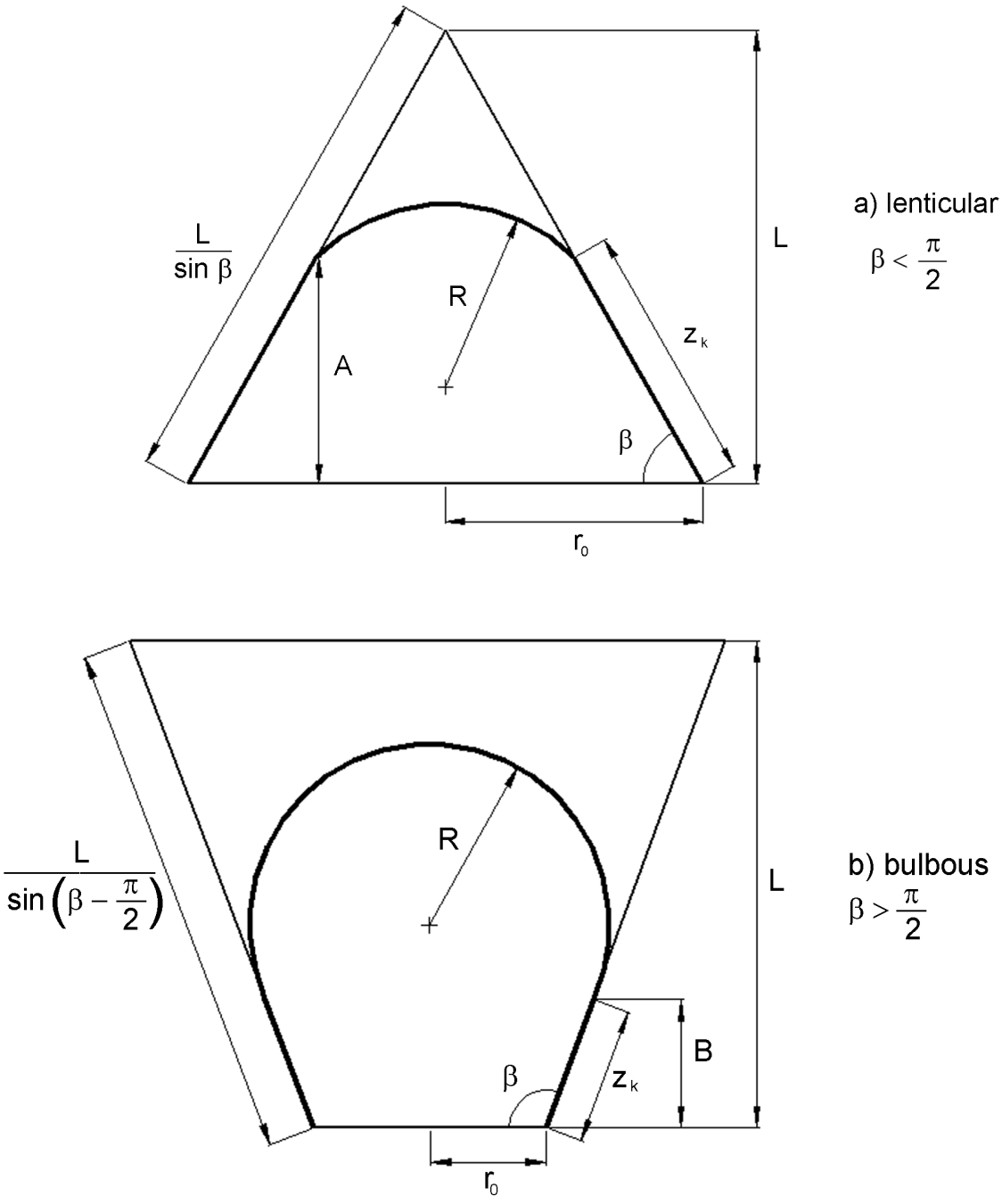

Figure 5: Dimensional schematic of transitioning cone ($\mathrm{A} \equiv z_k \sin\beta$ *and* $\mathrm{B} \equiv z_k \sin\left(\beta - \frac{\pi}{2}\right)$*)*

To get the thickness profile, we substitute (50) into (47):

since $T_0 \equiv 1$

$$T = \frac{1}{2}(1+\cos\beta)\left(1-\frac{Z_\kappa}{2\ell}\sin\beta\right)^{\sec\beta-1} \tag{51}$$

combining (43) and (51)

$$T = \frac{1}{2}(1+\cos\beta)\left(\frac{\sin^2\beta}{2\ell\cos\beta}\right)^{\sec\beta-1} \tag{52}$$

When β exceeds $\frac{\pi}{2}$, the constrained melt's shape changes from lenticular to bulbous [1, 4,5,9].

VI. Constrained Forming Results

Substituting (52) into (23)

$$\left|\frac{d\rho}{d\theta}\right| = \alpha\rho^{3-\sec\beta} \tag{53}$$

where the *cone shape factor* is

$$\alpha \equiv \frac{1+\cos\beta}{2\alpha_0}\left(\frac{\sin^2\beta}{2\ell\cos\beta}\right)^{1-\sec\beta} \tag{54}$$

where Table 3 defines the dimensionless cone height, 2ℓ (Figure 5 defines the cone height, L). When $\beta < \frac{\pi}{2}$, a lenticular cap progresses down the cone. Hence,

$$\frac{d\rho}{d\Theta} = \alpha\rho^{3-sec\,\beta};\ \beta < \frac{\pi}{2} \tag{55}$$

Integrating gives

$$\Theta = \frac{\rho^{sec\,\beta-2}}{\alpha(sec\,\beta-2)};\ \frac{\pi}{2} > \beta \neq \frac{\pi}{3} \tag{56}$$

and

$$\Theta=\frac{\log(\rho)}{\alpha}\ ;\beta=\frac{\pi}{3} \tag{57}$$

For thermoforming with $\beta>\frac{\pi}{2}$, a bulbous cap progresses down the cone. Hence,

$$\frac{d\rho}{d\Theta}=-\alpha\rho^{3-sec\,\beta}\,;\beta>\frac{\pi}{2} \tag{58}$$

and integrating gives

$$\Theta=\frac{-\rho^{\sec\beta-2}}{\alpha(sec\,\beta-2)}\,;\beta>\frac{\pi}{2}\neq\frac{4\pi}{3} \tag{59}$$

and

$$\Theta=\frac{-\log(\rho)}{\alpha}\ ;\beta=\frac{4\pi}{3} \tag{60}$$

Linearizing (56) gives

$$ln\,\rho=\left(\frac{1}{sec\,\beta-2}\right)ln\Theta+\frac{ln\left(\alpha(sec\,\beta-2)\right)}{(sec\,\beta-2)}\,;\beta\neq\frac{\pi}{3} \tag{61}$$

and linearizing (59):

$$ln\,\rho=\left(\frac{1}{\sec\beta-2}\right)ln\Theta+\frac{ln\left(\alpha(2-sec\,\beta)\right)}{(\sec\beta-2)}\,;\beta\neq\frac{4\pi}{3} \tag{62}$$

Hence, zero radius of curvature takes an infinite period of constrained forming. In other words, the melt will never reach the cone apex, and Z_κ never reaches 1. Thus, Eqn. (61) and (62) explain why sharp corners are difficult to thermoform. The thermoforming of sharp edges or corners is called **detailing**.

Letting ρ_f be the desired dimensionless **apex sharpness**, we then get:

$$\Theta_f = \left|\Theta(\rho_f) - \Theta(\rho_\kappa)\right| \tag{63}$$

for the required constrained forming interval. Thus, the total manufacturing time is

$$\begin{aligned}\theta_T &= \theta_\phi + \Theta_f \\ &= \theta_\phi + \left|\Theta(\rho_f) - \Theta(\rho_\kappa)\right|\end{aligned} \tag{64}$$

For the melt, the stress is

$$\Sigma_{\phi\phi} = \frac{-\alpha\rho^{1-\sec\beta}}{6}; \beta < \frac{\pi}{2} \tag{65}$$

which linearizes to

$$\ln\left(\frac{\Sigma_{\phi\phi}}{\alpha}\right) = (1-\sec\beta)\ln\rho + \ln\left(\frac{-1}{6}\right) \tag{66}$$

and

$$\Sigma_{\phi\phi} = \frac{\alpha\rho^{1-\sec\beta}}{6}; \beta > \frac{\pi}{2} \tag{67}$$

which linearizes to

$$\ln\left(\frac{\Sigma_{\phi\phi}}{\alpha}\right) = (1-\sec\beta)\ln\rho + \ln\left(\frac{1}{6}\right) \tag{68}$$

VII. Plug Assist

In thermoforming, plug assist is often used to even out wall thickness profiles. Figure 6 illustrates the variables for plug-assisted thermoforming.

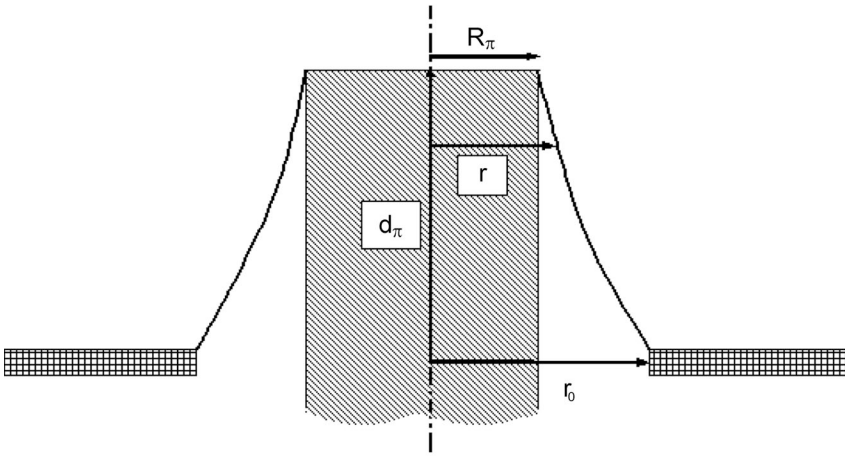

Figure 6: Plug assist

Our work focused on unassisted thermoforming, and thus derives the worst case for wall thickness variation. We define the final wall thickness uniformity as:

$$\Upsilon \equiv \frac{h(z_{\kappa f})}{h(z_{\kappa}=0)} = \frac{T(Z_{\kappa f})}{T(Z_{\kappa}=0)} \tag{69}$$

where $z_{\kappa f}$ is the final contact length, corresponding to the final desired radius at the cone tip:

$$Z_{\kappa f} = \frac{2\ell}{\sin\beta} - \rho_f \tan\beta \tag{70}$$

Combining (51) with (69) gives:

$$\Upsilon \equiv \left(1 - \frac{Z_{\kappa f}\sin\beta}{2\ell}\right)^{\sec\beta - 1} \tag{71}$$

and substituting (70) into this yields:

$$\Upsilon \equiv \left(\frac{\rho_f \sin\beta \tan\beta}{2\ell}\right)^{\sec\beta - 1} \tag{72}$$

and in the limit, for an infinitely sharp cone tip, we get:

$$\Upsilon \equiv \left(1-\frac{1}{2\ell}\sin\beta\right)^{\sec\beta-1} \tag{73}$$

which is the **worst case** for the cone thickness uniformity. Equations (71) and (72) dictate just how much plug assist is required to even out the cone wall thickness distribution. Equation (73) gives the upper bound for this plug assist requirement.

From the geometry of the deformation, and in cylindrical coordinates, Williams derived the following for the thickness profile caused by plug assist

$$T \equiv \frac{1}{\sqrt{1+\left(\frac{d_\pi}{r\ln\frac{r_0}{R_\pi}}\right)^2}} \tag{74}$$

and verified this experimentally. This adimensionalizes to

$$T \equiv \frac{1}{\sqrt{1+\left(\frac{2}{\frac{\omega}{\sigma\ell}\ln\frac{1}{\alpha_\pi}}\right)^2}} \tag{75}$$

where σ is the dimensionless plug displacement (normally called stroke), α_π is the plug shape factor and ω is the center line proximity. So during plug assist, the deforming melt's thinnest part is near the plug's edge where:

$$T_{min} = \frac{1}{\sqrt{1+\left(\frac{2}{\frac{\alpha_\pi}{\sigma\ell}\ln\frac{1}{\alpha_\pi}}\right)^2}} \tag{76}$$

and its thickest, near the mold rim, where:

$$T_{max} = \frac{1}{\sqrt{1+\left(\dfrac{2}{\dfrac{1}{\sigma\ell} ln \dfrac{1}{\alpha_\pi}}\right)^2}} \tag{77}$$

In principle, we would like to match the severity of the cone thickness problem, Υ, with the amount of plug assistance near the rim, T_{max}. In practice, however, the plug normally runs into the cone before this amount of plug assistance can be realized. To prevent this, the stroke must satisfy this geometric inequality:

$$\sigma < \frac{\alpha_0}{2\ell}\left[\frac{(1-\alpha_\pi)\,tan\,\beta}{\alpha_0} - 1\right] \tag{78}$$

For a right cylinder, where $\beta = \dfrac{\pi}{2}$, the plug can never run into the mold; Throne has outlined an approach for this special case [6].

VIII. Worked Examples

A. Process speed and melt stress

A plastics engineer wants to manufacture a safety cone with $\beta = 75.5°$ and $L = 31\,\text{cm}$ from a disk of uniform thickness $h_0 = 1.51\ \text{mm}$ and from a nearly Newtonian melt with $\mu = 3.11\times10^6\ \text{Pa}\cdot\text{s}$. She desires a blunt cone of apex radius, $R_f = 25.4\ \text{mm}$. She employs an external gage pressure of $91.3\ \text{psi}$ and a vacuum of $14.1\ \text{psi}$. Calculate the total forming time, and estimate the stress frozen into the safety cone, both near its rim and into its blunt tip.

Using Table 3, we calculate $\ell \equiv (tan\,\beta)/2 = 1.93$. Substituting into (44) gives a dimensionless radius of curvature of $\rho_\kappa = 1.03$ when constrained forming begins. Substituting this and $\alpha_0 \equiv h_0 / r_0 = 0.0188$ (from Table 3) into (45) then gives a dimensionless free forming time of $\theta_\phi = 1.85\times10^{-3}$. Combining $\rho \equiv R / r_0$ from Table 3 with $r_0 \equiv L / tan\,\beta$ from Table 3 gives the dimensionless radius of curvature of the blunt cone tip $\rho_f \equiv R_f / r_0 = 0.312$. Substituting θ_ϕ, ρ_κ, $\rho_f \equiv R_f / r_0 = 0.312$ and $\alpha \equiv (\sin^2\beta / 2\alpha_0(1-\cos\beta))\left(\sin^2\beta / 2\ell\cos\beta\right)^{1-\sec\beta} = 36.4$ into (64) gives a total dimensionless forming time of $\theta_T = 0.015$.

Summing the vacuum and the applied air pressures gives $\Delta P = 105.4$ psi. Using this and Table 3, we find the total-forming time of $t_T = 12\mu\Theta_T / \Delta P = 0.770$ s. We then substitute ρ_κ, and $\alpha = 36.4$, into (65) to obtain the dimensionless stress near the rim of $\Sigma_{\phi\phi}\big|_{rim} = -6.65$, which is tensile. We expect most of this to freeze into the rim. Using Table 3, we find that this corresponds to a tensile stress at the rim of $\Sigma_{\phi\phi}\big|_{rim}\,\Delta P = \tau_{\phi\phi}\big|_{rim} = -5.53$ MPa, which is also tensile.

Substituting ρ_f, and α into (65) gives the dimensionless stress near the blunt tip of $\Sigma_{\phi\phi}\big|_{tip} = -253.7$, which is tensile. We expect most of this to freeze into the tip. Using Table 3 we find that this corresponds to a tensile stress at the rim of $\Sigma_{\phi\phi}\big|_{tip}\,\Delta P = \tau_{\phi\phi}\big|_{tip} = -211$ MPa.

B. Pressure difference and part height

A plastics engineer wants to process the same safety cone as in Example A, but his process economics require a forming time to fall below 1.2 seconds. Find the required ΔP, finished part height, and estimate the stress frozen into the safety cone, both near its rim and into its blunt tip.

Using $\theta_T = 0.015$ from Example A, for the required applied pressure difference we find $\Delta P = 12\Theta_T \mu / t = 67.7$ psi. From the cone geometry, for the finished part height we get:

$$H_p = \sin\beta\left(\frac{L}{\sin\beta} - R_f \tan\beta - \frac{R_f}{\tan\beta}\right) + R_f \tag{79}$$

which gives 0.24 m.

C. Cone sharpness

A plastics engineer wants to manufacture a pointy cone $(\rho_f \approx 1)$ with $\beta = 75.5°$ and $L = 0.31\,\text{m}$ from a disk of nearly Newtonian melt with $\mu = 3.11\times10^6\ \text{Pa}\cdot\text{s}$ and uniform thickness $h_0 = 1.51$ mm. She employs an external gage pressure of $91.3\,\text{psi}$ and a vacuum of $14.1\,\text{psi}$. Her mold has an infinitely sharp cone tip, and she employs a long forming time, $t_T = 10\,\text{s}$. Calculate the resulting apex radius.

Summing the vacuum and the applied air pressures gives $\Delta P = 105.4$ psi. Using this and Table 3, we find the total-dimensionless forming time of $\Theta_T = \Delta P t_T / 12\mu = 0.194$. Using Table 3, we calculate $\ell \equiv (\tan\beta)/2 = 1.93$, and substituting into (44) gives a dimensionless radius of curvature when constrained forming begins of $\rho_\kappa = 1.03$.

Substituting this and $\alpha_0 \equiv h_0 / r_0 = 0.0188$ (from Table 3) into (45) then gives a dimensionless free forming time of $\theta_\phi = 1.85 \times 10^{-3}$. Combining ρ_κ, Θ_T and θ_ϕ into (64), and solving for the dimensionless apex radius gives:

$$\rho_f = \left(\alpha(sec\,\beta - 2)\left(\theta_T - \theta_\phi\right) + \rho_\kappa^{sec\,\beta - 2}\right)^{\frac{1}{sec\,\beta - 2}} \tag{80}$$

Using this and Table 3 we get $\rho_f = 3.89$ and thus find the cone tip sharpness to be $R_f = \rho_f r_0 = 31.2$ cm.

D. Plug assist

A plastics engineer wants to process the same safety cone as in Example A, but in this case, she wants a more uniform wall thickness distribution. For this she employs plug assist, specifically using a right cylindrical plug with $R_\pi = r_0 / 2 = 4.01$ cm with a plug displacement of 13.8 cm. Estimate the improvement in wall thickness uniformity.

Combining $\rho \equiv R / r_0$ from Table 3 with $r_0 \equiv L / tan\,\beta$ from Table 3 gives the dimensionless radius of curvature of the blunt cone tip $\rho_f \equiv \left(R_f\, tan\,\beta\right) / L = 0.312$. Since $R_\pi = r_0 / 2$, the dimensionless cone shape factor is $\alpha_\pi \equiv R_\pi / r_0 = 1/2$. Using Table 3, we calculate $\ell \equiv (tan\,\beta) / 2 = 1.93$, and substituting this and ρ_f into (72) gives the sheet uniformity, $\Upsilon = 0.0279$. This is the uniformity that would be obtained without plug assist.

Using Table 3 , we calculate a stroke of $\sigma \equiv d_\pi / L = 0.446$. Substituting into (77) gives $T_{max} = 0.373$. This means that the melt cone's rim will begin free forming at a thickness

that is 62.7% of the disk's initial thickness. We thus expect the plug assist to improve the uniformity to:

$$\Upsilon_{\pi} \cong \frac{\Upsilon}{T_{max}} = 0.0748 \tag{81}$$

which corresponds to roughly a three-fold improvement in cone wall thickness uniformity.

IX. Conclusion

This new analysis for thermoforming cones focuses on the manufacturing process speed. Specifically, we've distinguished between what happens before (free forming) and after (constrained forming) the melt touches the conical mold. We derive the time required for both cases, and sum them to get the total forming time. We've restricted our analysis to the Newtonian case and adimensionalized our results at every step. For free forming, one dimensionless geometric shape factor arises (α_0), and for constrained, two arise (α and $\sec\beta$). We also calculate the stresses in the deforming melt, since these govern the residual stresses in the thermoformed part. We then derive an expression for wall uniformity; we find that it just depends on the mold geometry. Finally, we attack the problem of plug assist, deriving an expression for the improvement in wall uniformity achieved through plug assist.

X. Acknowledgement

The authors are indebted to Dr. Zhongbao Chen of the University of Wisconsin and to Dr. Martin J. Stephenson of the Placon Corporation for their invaluable advice. We further acknowledge Professor R. Byron Bird for his help with the thin film

approximation. We thank the Placon Corporation of Madison, Wisconsin and Plastic Ingenuity, Inc. of Cross Plains, Wisconsin for their financial support through their memberships in the Industrial Consortium of the Center for Advanced Polymer and Composite Engineering at the University of Wisconsin. The Placon Corporation is also recognized for its sustaining sponsorship of the Rheology Research Center.

Appenix : Thin Film Approximation

Here we explore the virtue of the thin film approximation. Eliminating the stresses in equation (15) gives

$$\Delta P = \int \frac{2\mu R^2 \left|\dot{R}\right| + 2\mu R^2 \left|\dot{R}\right| - 8\mu R^2 \left|\dot{R}\right|}{r^4} dr = \int \frac{-4\mu R^2 \left|\dot{R}\right|}{r^4} dr \tag{82}$$

Thus,

$$\Delta P = -4\mu R^2 \left|\dot{R}\right| \int_R^{R+h} \frac{dr}{r^4} = 12\mu R^2 \left|\dot{R}\right| \left[\frac{1}{(R+h)^3} - \frac{1}{R^3} \right] \tag{83}$$

Using Table 3, this adimensionalizes to:

$$\left|\frac{d\rho}{d\theta}\right| = \left[\frac{\rho(\rho + T\alpha_0)^3}{-(\rho + T\alpha_0)^3 + \rho^3} \right] \tag{84}$$

Though this is more accurate than (23), neither substituting (24) or (26) into (84) for free forming, nor (52) into (84) for constrained forming, leads to differential equations having analytical solutions. This is why thermoforming analysis relies so heavily on the thin film approximation.

Part II: Thermoforming Cups

Abstract

Although research has been conducted for more than twenty years on finite element simulations of the thermoforming process, most developments only concentrate on vacuum forming. In addition, most studies model the simulated polymers as elastic solids that remember their original state, and return to it if reheated after initial forming. In reality, they are actually viscoelastic fluids that do not retain a memory of their original shape. Furthermore, the use of plug assist has not been deeply explored. This work focuses on using POLYFLOW finite element simulation software to accurately predict the material thickness of plug assisted vacuum formed polypropylene copolymer cups for an existing manufacturing process. The simulation inputs accurately model the current process, duplicating processing conditions and the material rheological parameters as a viscoelastic fluid. The processing conditions considered include the plug and mold shapes, pressure, temperature and plug draw depth. The rheology is obtained from a previous characterization of this polypropylene [25]. The simulation accuracy is determined by comparing predicted thicknesses with measured values from the manufacturing operation and lab. Once the model is accurately simulated, changes are made to processing conditions to improve thickness uniformity and increase minimum thickness in order to prevent hole formation in the plastic. The results show that a simplified material characterization is the most accurate processing simulation. Furthermore, the process is improved with a deeper draw depth.

I. Introduction

A vacuum formed thermoforming process consists of a thermoplastic heated above its glass transition temperature and formed into a mold with the application of a pressure vacuum. This process is widely used to manufacture many of the plastic products we use today. Some common examples are rigid plastic food containers and consumer product packaging. There are limits to the depth of a thermoplastic container with vacuum forming alone, therefore a plug assist is used to increase the product depth, or draw ratio. Plug assist is used to prestretch the material before vacuum pressure is applied to complete the thermoforming process. Depending on the amount the plug stretches the melt, or draw depth, different wall thickness distributions are obtained.

Analytical solutions for wall thickness have been developed for constrained thermoforming by Rozenzweig [15], considering the polymer as an elastic solid. Finite element, analytical and experimental results were compared by Charrier [16] with the polymer as an elastic solid in free and constrained thermoforming. Basic shapes considered were tubes, plates and cones. Throne [17] and Williams [4] also developed analytical wall thickness solutions for constrained thermoforming, as well as for plug assisted thermoforming into cones. These solutions considered the polymer as an elastic solid. Williams compared his analytical solution for truncated cones with experimental work with polymethylmethacrylate (PMMA) and found good agreement. These experimental results were used by Song [18] to compare with a finite element program for plug assisted thermoforming of cones, simulating the polymer as an elastic solid. Song also calculated thickness profiles with a finite element program for a truncated cone

of PMMA. DeLorenzi [19] compared thickness profiles calculated using a finite element program with experimental results for high impact polystyrene (HIPS). An elastic approach was used for constrained forming into a rectangular and cylindrical mold. The rectangular mold used both *straight thermoforming*[2] and plug-assisted thermoforming. A non-isothermal temperature model was found to be most accurate for the cylindrical mold. Nied [20] developed a finite element program for straight thermoforming of Acrylonitrile butadiene styrene (ABS), and compared the calculated thicknesses with experimental results. Erchiqui (2004) [21] developed a finite element program for ABS using an elastic solid approach to free inflation, calculating stress and bubble height. He also used an elastic approach to develop a program for a straight thermoformed rectangle. These calculations were compared with a linear viscoelastic model, using the Lodge-Maxwell equation.

Most of the focus for finite element simulations of thermoforming has been on elastic solid material behavior. However, Erchiqui 2005 [22] developed a viscoelastic finite element program for straight thermoforming of high density polyetheylene (HDPE) using the Wagner model for a nonlinear model, and the Lodge-Maxwell equation for the linear model. Temperature dependence of viscosity was governed by the WLF equation. Stretch, strain and thickness were calculated for a rectangular mold and compared with experimental results. Lee [23] calculated thickness for a complex mold with a viscoelastic finite element program and compared the results with experiments. Prestretching was applied with an initial vacuum pressure, before pressure was applied in the reverse direction. The simulation used the Wagner equation as a nonlinear model,

[2] Also known as vacuum forming.

and explored the effect of elongational and extensional parameters in the Wagner equation for polymer forming into a tube. The thickness distribution changed with sheet temperature and mold temperature, Bubble shape was effected by variation of the elongational and deformation resistance terms of the nonlinear model.

There is a gap in the research for viscoelastic simulations of polypropylene for both straight and plug assisted thermoforming. Therefore, this work is significant to the field as the first comparison between experimental and calculated thickness results for plug assisted simulations for polypropylene copolymer. The simple shape of a truncated cone is used to study the accuracy of the linear model using the Lodge-Maxwell equation, and the nonlinear model using the Wagner equation. Furthermore, the effect of α and β parameters from the Wagner equation, as well as plug temperature variations will be studied. Previous research has also never investigated the effect of the amount of prestretching, accomplished with plug assist and increased with draw depth, on the final part thickness. Therefore, this work will be the first to explore variations in prestretching.

II. Finite Element Procedures

The purpose of this analysis is to model the actual processing conditions and validate the use of this finite element program to accurately predict final thickness distributions. Once an accurate model is established, the primary purpose is to investigate the effects of variations in material characterization, sheet prestretching, sheet temperature, and shear

behavior. These investigations can be used to improve an existing process by increasing both thickness uniformity along the cup sides, and to engineer the minimum thickness.

For the simulations, the polymer is assumed to be incompressible, isotropic and a non-isothermal thin film. Furthermore, the plug and mold are both isothermal. The POLYFLOW finite element simulation software version used was 3.10.4 .

A. Cup Specifications

Our cup is manufactured from polypropylene and is made by a plug assisted vacuum formed thermoforming operation. Because of the cylindrical shape it is symmetric along its centerline.

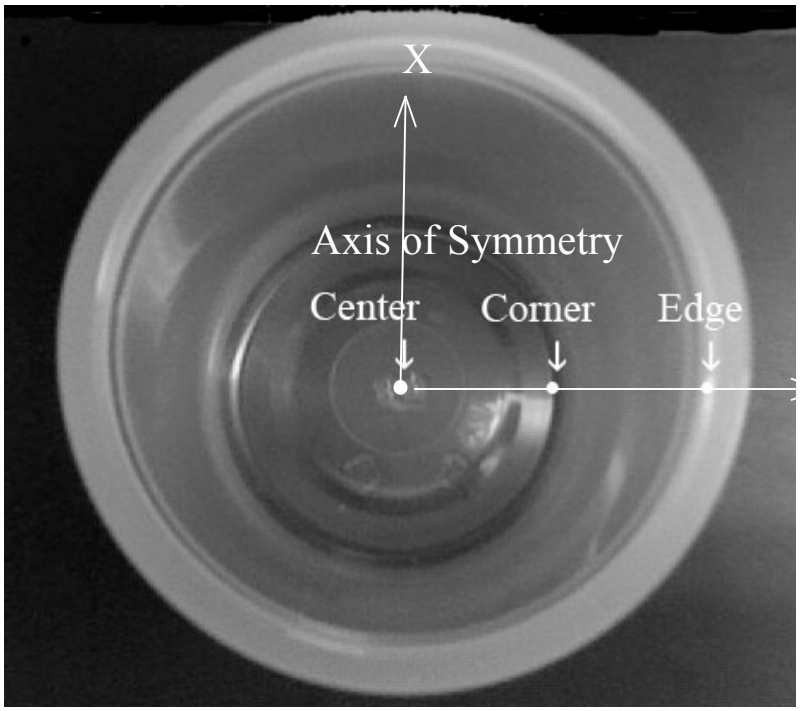

Figure 7: Cup with labeled axis

B. Plug Assisted Model

The simulation takes advantage of the cylindrical symmetry about the cup centerline. We simulate the plug assisted thermoforming of one quarter of the total volume, as shown in Figure *8*.

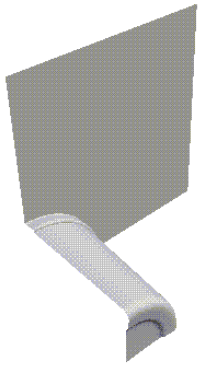

Figure 8: Simulated Cup

The process begins with a thin, flat polymer sheet of uniform thickness resting on a flat mold surface (Figure 9). A fine mesh is used to provide sufficient details of the cup shape as it forms into the tight edges in the mold corners. A cylindrical plug with a rounded tip pushes down on the sheet center; this prestretches the material before any vacuum pressure is applied (Figure 10). With the exception of the material contacting the plug and top flat mold surfaces, the sheet thins. The simulation maintains the initial sheet thickness at the flat mold surface, where the cup edge rests, for the entire process. After sufficient prestretching, vacuum pressures is applied to inflate the sheet into the unheated mold (Figure 11). As the sheet touches the mold's sides, its shape freezes immediately

(Figure 12). The total forming time is around 1.02 seconds. The newly formed cup is left in the mold for an additional second to cool the cup.

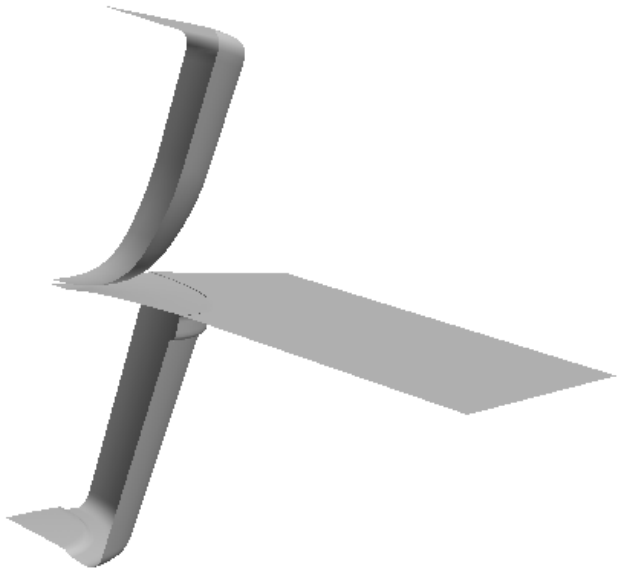

Figure 9: Initial position of polymer sheet, plug and mold before any contact occurs.

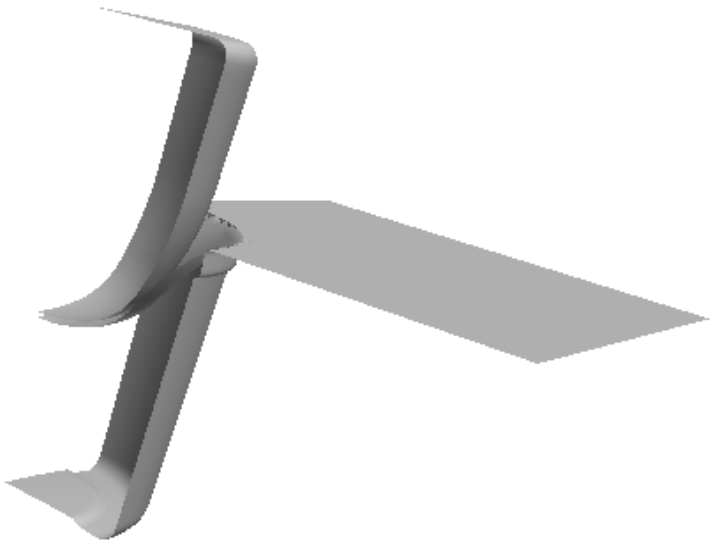

Figure 10: Plug stretching the polymer sheet. The sheet has not yet touched the mold.

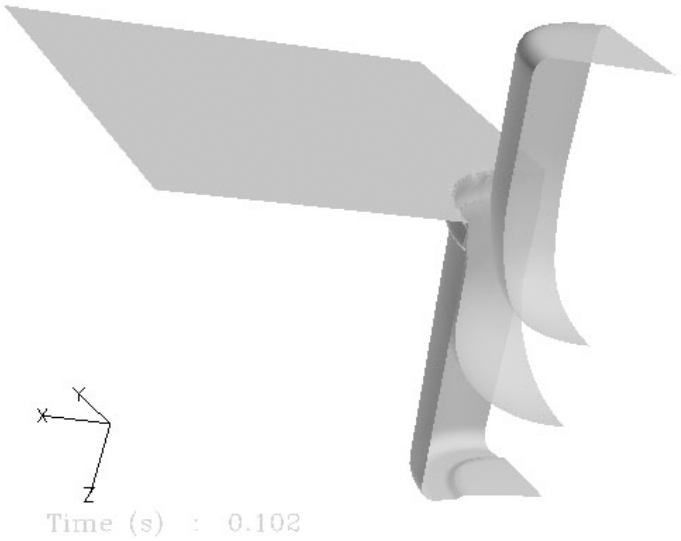

Figure 11: Screenshot taken as the sheet is inflated. It is no longer touching the plug and just beginning to touch the mold at the top. The total plug contact time is 1.02 s.

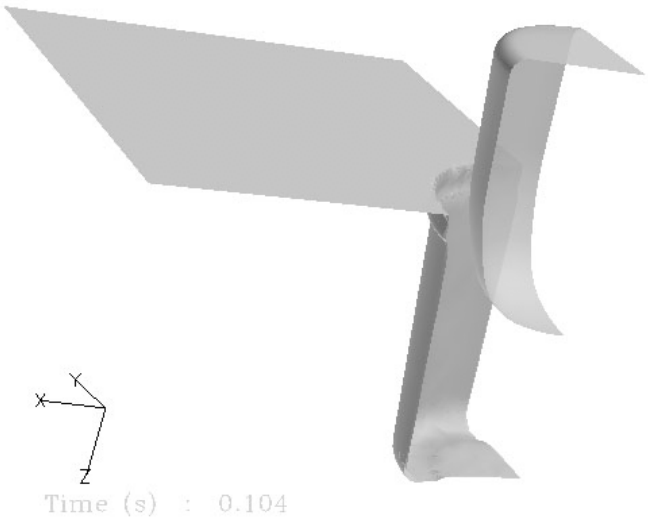

Figure 12: Final sheet position just after the after it freezes into position in the mold. The total mold contact time is 0.02 s.

The process described above for the simulation matches the manufacturing operation. The real mold contains several cups thermoformed at once, much like a cupcake pan. After the thermoforming process is completed with this multi cup mold, the edges must be cut to create individual cups in a trimming operation. This process is not simulated by the program, and consists of a die compressing the cup edge at the flat mold surface as it cuts the circular edge. Figure 7 shows this. Because the edge is compressed, the measured edge thickness subceeds the simulation's calculated edge thickness.

C. Viscoelastic Models

The nonlinear viscoelastic results use the irreversible Wagner model, which accounts for the *net disentanglement* of polymer chains during flow. This induces nonlinearity in the shear and elongational polymer behaviors. The irreversible Wagner model accurately describes these behaviors. Linear viscoelastic results are obtained with the special case called the Lodge-Maxwell model, where no net disentanglement occurs.

1. Nonlinear Function

For the Wagner model the viscoelastic component of the total extra stress tensor component, T, is

$$T = \frac{1}{1-\theta}\int_0^{\infty}\sum_{i=1}^{N}\frac{\eta_i}{\lambda_i^{\,2}}\exp\left(\frac{-s}{\lambda_i}\right)H(I_1,I_2)\left[C_t^{-1}(t-s)+\theta C_t(t-s)\right]ds \tag{85}$$

where i indicates which relaxation modes, with η_i and λ_i as its corresponding viscosity and relaxation time; (η_i, λ_i) is called the discrete relaxation spectrum, where λ_i varies with temperature, T, as:

$$\lambda_i = a_T \lambda_{id} \tag{86}$$

where λ_{id} is the discrete relaxation time of the ith mode. T_d is the temperature at which the spectrum was measured [25]. For our polypropylene:

$$T_d = 463K \tag{87}$$

a_T is calculated from the WLF equation, given by

$$\ln a_T = \frac{C_1(T_r - T_d)}{C_2 + T_r - T_d} - \frac{C_1(T - T_d)}{C_2 + T - T_d} \tag{88}$$

where C_1 and C_2 are universal WLF constants

$$\begin{aligned} C_1 &= 8.86\ K \\ C_2 &= 101.6\ K \\ T_r &\equiv T_g + 50K \end{aligned} \tag{89}$$

corresponding to the reference temperature:

$$T_r \equiv T_g + 50K \tag{90}$$

where T_g is the glass transition temperature. For polypropylene [25]:

$$T_g = 263K \tag{91}$$

Furthermore, in Eq. (85) the current time is t and the interval since past time t' with respect to t is s. Lastly, C_t is the Cauchy-Green strain tensor, H, the damping function described below, and θ is a normal stress scalar, defined as

$$\theta \equiv \frac{N}{1+N} \tag{92}$$

where the normal stress difference ratio N is

$$N \equiv \frac{N_2}{N_1} \tag{93}$$

with N_1 and N_2 being the first and second normal stresses. For the PSM model [26], the damping function H is:

$$H = \frac{\alpha}{\alpha + (I - 3)} \tag{94}$$

where α is the entanglement resistance to deformation. Additionally, I is the unit tensor represented by

$$I = \beta I_1 + (1 - \beta) I_2 \tag{95}$$

where β governs the sensitivity of biaxial or uniaxial extensional behaviors to the first invariant of the Cauchy-Green strain tensor, I_1. Whereas α varies from one polymer to the next, for most polymer melts, β is

$$\beta = \frac{1}{50} \tag{96}$$

Hence, biaxial or uniaxial behaviors are dominated by I_2 and only weakly dependent on I_1.

2. Linear Function

For the Lodge-Maxwell model the total extra stress tensor, T, is

$$T = \int_0^{\infty} \sum_{i=1}^{N} \frac{\eta_i}{\lambda_i^2} \exp\left(\frac{-s}{\lambda_i}\right) \left[C_t^{-1}(t - s)\right] ds \tag{97}$$

which is just the Wagner model [(85)] with:

$$H = 1 \; ; \theta = 0 \, . \tag{98}$$

D. Material Characterization

1. Discrete Relaxation Spectrum

The discrete spectrum is composed of five previously measured values Hade and Giacomin [24] obtained from their rheological measurements at 463 K :

Mode	η_i (Pa-s)	λ_i (s)	G_i (Pa)
1	216.7	0.000788	275,000
2	1136	0.03792	29,960
3	1549.3	0.1657	9,350
4	1566.5	0.6468	2,422
5	10928.2	6.234	1,753

Table 4: Discrete Spectrum

2. Single Relaxation Time Calculation

Letting

$$G_i \equiv \frac{\eta_i}{\lambda_i} \tag{99}$$

define the relaxation modulus of the i th mode, we now let:

$$\bar{G} \equiv \sum x_i G_i \tag{100}$$

define our average relaxation modulus, where

$$x_i \equiv \frac{G_i}{\sum G_i} \equiv \frac{G_i}{G_T} \tag{101}$$

so that

$$\bar{G} = \frac{\sum G_i^2}{G_T}. \tag{102}$$

We then want η_0 for both our single and multiple relaxation time fluids to match. For a Maxwell fluid:

$$\eta_0 = \sum G_i \lambda_i \tag{103}$$

and for our single relaxation time fluid:

$$\eta_0 = \bar{G}\bar{\lambda} \tag{104}$$

Combining [(103)] and [(104)] we find the following for our average relaxation time

$$\bar{\lambda} = \frac{\sum G_i \lambda_i}{\bar{G}} \tag{105}$$

Combining this with [(102)], we get:

$$\bar{\lambda} = \frac{G_T \sum G_i \lambda_i}{\sum G_i^2} \tag{106}$$

Eqns. (103) and (105) are used in our simulations for the single relaxation time fluid.

Variable	**Value**
η_0	69,400 Pa-s
$\bar{\lambda}$	0.117 s
G_T	15.4 kPa
$\sum G_i^2$	126 MPa^2
$\bar{G}$	8.16 kPa

Table 5: Calculated values for single relaxation time fluid.

E. Plug Heat Transfer

Heat transfer to the mold solidifies the part, without affecting its wall thickness distribution. However, heat transfer to the plug can reshape the part. Plug heat transfer is implemented by varying the plug temperature, without changing the melt temperature. The dimensionless temperature difference, θ is

$$\theta \equiv \frac{T_s - T_p}{T_s - T_m} \tag{107}$$

A value of zero indicates that there is no heat transfer to the plug.

F. Simulation Variation

The Table 6 summarizes the processing conditions and material parameters used in the simulation and Table 7 summarizes the simulations.

Parameter	Value (if constant)	Constant	Variable
Mold Temperature	295 K	x	
Plug Temperature	433 K	x	
Plug Speed	0.254 m/s	x	
Inflation Pressure	5000 Pa	x	
β		x	
Sheet Temperature			x
α			x

Table 6: Material parameters and processing conditions.

Simulation #	Multiple Relaxation	Single Relaxation	Linear Viscoelastic	Nonlinear Viscoelastic	α	Plug Temperature (K)	θ	β	Plug
1.	x		x		-	433	0	-	-
2.		x	x		-	433	0	-	-
3.		x		x	0.12	433	0	0.02	-
4.		x		x	0.11	433	0	0.02	-
5.		x		x	0.1	433	0	0.02	-
6.		x		x	0.12	433	0	0.02	-
7.		x		x	0.12	433	0	0	-
8.		x	x		-	440	-0.051	-	-
9.		x	x		-	420	0.094	-	-
10.		x	x		-	400	0.239	-	-
11.		x	x		-	433	0	-	A
12.		x	x		-	433	0	-	B
13.		x	x		-	433	0	-	C

Table 7: Material parameters and processing conditions.

III. Experimental Procedures

A. Plant and Laboratory Data

Measurements are taken periodically at the manufacturing site for quality control purposes. The thicknesses of the polypropylene are taken at eight locations along the bottom, side and top of the cup. The Magna-Mike 8000 was used to obtain all the data.

A calibration using the Magna-Mike calibration apparatus was performed before each new measurement for maximum accuracy. In the laboratory additional measurements were taken along the cup contour with a Magna-Mike 8000. The calibration apparatus was also used before each new measurement.

B. Method for Comparison of Simulation and Data

Because of the cup's symmetry, only one half of the cup was used for comparison. A contour was calculated from coordinate locations on the cup for both the simulation and data. The contour begins at the bottom center of the cup and extends along the centerline up the wall to the top edge.

IV. Results

Figure 13 shows the simulation results using both the single and multiple relaxation times, as discussed in the methods. These results are compared with process data and lab measurements, both shown with points.

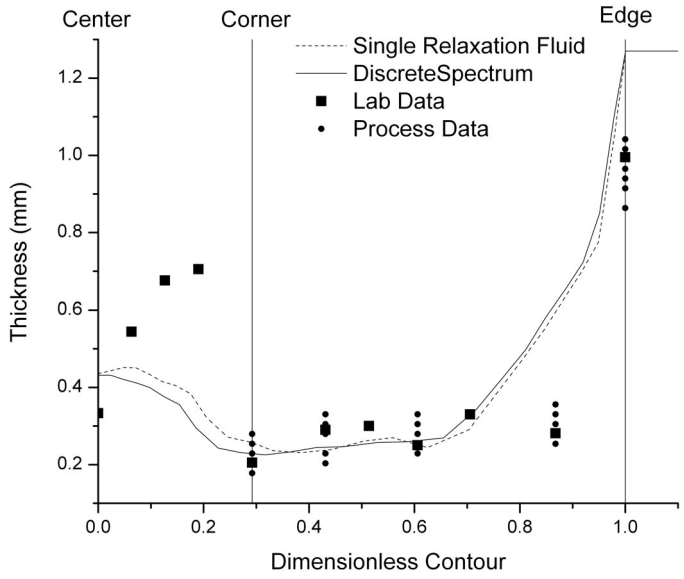

Figure 13: Simulation comparison with data for discrete spectrum and single relaxation time fluid.

The cup center, corner and edge locations are indicated on Figure 8. Along the bottom, between the center and corner, neither simulation shows a close fit with lab measurements. The main area of concern is the thinnest area, due to the possibility of rupture. For thermoformed cups, the thinnest part is the corner. Here both simulations are accurate. Along the sidewall both simulations over estimate thickness, however the single relaxation time fluid is the closest to data. Edge thickness for the simulations and process data disagrees by as much as 21 percent of the simulation edge thickness. This is due to the cutting operation, which compresses the initial material thickness and is not simulated with our finite element program. Overall, the single relaxation fluid fits the data at more points than the spectrum. Because the single relaxation time fluid is the most accurate we will use it to improve the existing process to obtain a larger minimum thickness and improve thickness uniformity along the cup bottom.

The accuracy of the single relaxation time fluid simulation is exciting. Whereas the spectrum consumed 8011.6 sec of CPU time, the single relaxation time computation consumed only 7166.1 sec. For more complicated shapes, bigger savings in computation time are expected. Furthermore, the use of single relaxation time fluids allows us to easily adimensionalize simulation results. Defining the Deborah and Weissenberg numbers, for example, is straightforward.

To improve the simulation's thickness uniformity at the bottom and sidewall areas, as well as to increase the minimum thickness, we have modified plug temperature, plug draw depth, and polymer entanglement resistance. Left to its own devices, the plug temperature will eventually reach a steady state, matching the melt temperature. If we

control the plug temperature, then raising it will transfer heat to the melt during plug assist. The heat transfer between the mold and sheet will always be insignificant because the polymer sheet freezes into place immediately upon contact with the mold. For this analysis the single relaxation time simulation was modified, because it had the best fit from Figure 13. Furthermore, the original single relaxation time simulation is displayed to detect any differences for new simulations. θ is the heat transfer value as described in the Methods section.

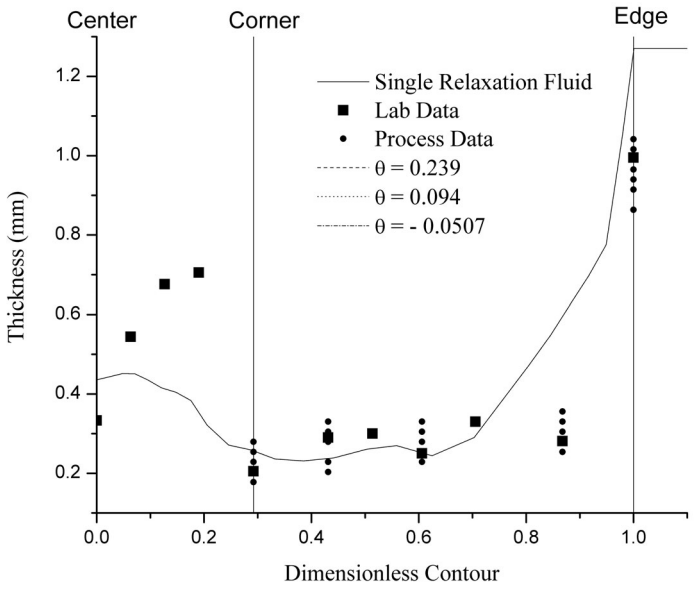

Figure 14: Effect of plug temperature.

Figure 14 shows no difference between the single relaxation time fluid with plug temperature changes. Therefore, the next parameter to vary is the plug draw depth, or prestretching, by the plug before the pressure is applied. The draw depth ratios are varied slightly. Figure 15 shows these results.

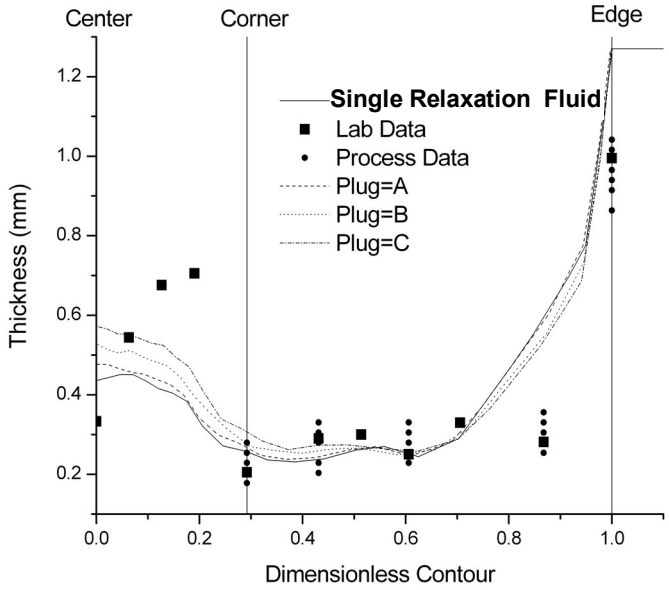

Figure 15: Effect of draw depth ratio.

As the draw depth increases from Plug A to Plug C, the sidewall area between the corner and edge decreases in thickness. The extra sheet material is pushed to the bottom between the center and corner. Also, the minimum thickness is increased as the draw depth increases.

The previous simulations have concentrated on the linear viscoelastic behavior. It is also necessary to explore the nonlinear viscoelastic behavior. This introduces a more complicated model, as described in the Methods. Figure 16 allows the exploration of changing the α to change the network strand's ability to resist deformation. A larger α value indicates an increased resistance.

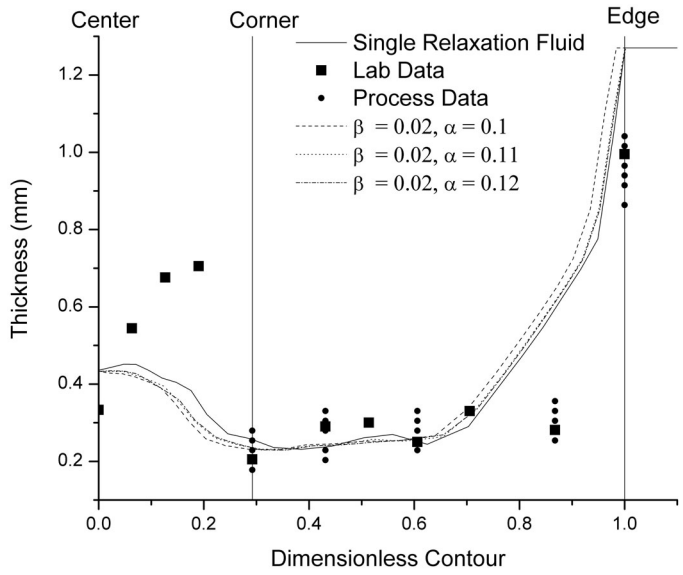

Figure 16: Effect of α for viscoelastic cases: nonlinear versus linear.

Overall, additional deformation resistance decreases the simulation accuracy. The linear model of the single relaxation time fluid is still the most accurate. This is especially evident at the sidewall between the corner and edge, and the bottom between the center and corner. As α decreases , the sidewall thickness and minimum thickness value decreases. Furthermore, edge thickness for the simulations and process data disagrees by as much as 21 percent. This is likely due to the difference between the processing simulation and the actual thermoforming process.

Figure 17 allows the exploration of changing the β to change the material's extensional behavior to I_1. A larger β value increases I_1.

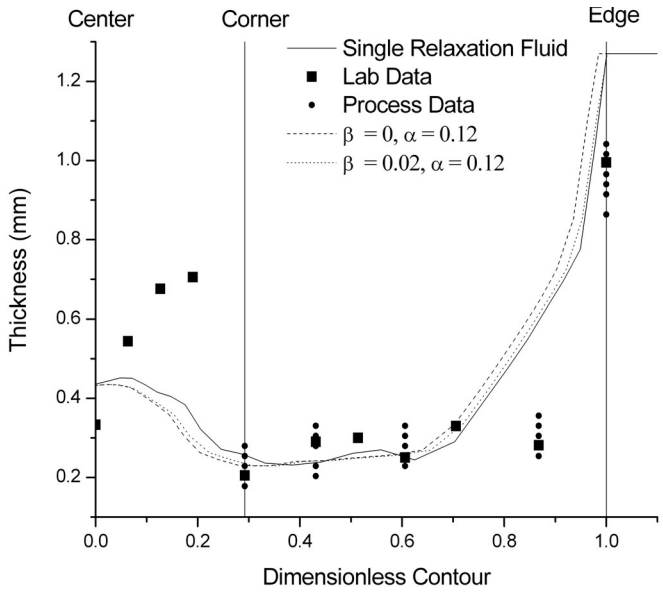

Figure 17: Simulation results from the β values for nonlinear viscoelastic.

Overall, the addition of extensional behavior to I_1 decreases the simulation accuracy. The linear model of the single relaxation time fluid is still the most accurate. This is especially evident at the sidewall between the corner and edge, and the bottom between the center and corner. As β decreases , the sidewall thickness and minimum thickness value decreases. Furthermore, edge thickness for the simulations subceeds the process data by as much as 21%.

V. Discussion

Because Figure 13 uses the actual processing conditions from the manufacturing environment, these results are used to validate the capability of this finite element program as method to predict the thickness distributions. Overall, the simulation follows the general pattern of the measured values and shows a desirable fit to measured values of the data points. This result validates the use of this finite element program to predict

the outcome of this specific cup thermoforming process. The literature also shows that finite element simulation provide good approximations to measured thicknesses for similar vacuum formed cross sections.

The simplified model of the single relaxation time fluid has a better fit to the data for a majority of the points, especially at the sidewall, corner and edge. Therefore, this is the best method characterize the polypropylene. This type of analysis has not been investigated in the literature. Previous literature has only analyzed the effect of processing conditions such as sheet temperature, mold temperature and the duration of pressure application.

Figure 13 also indicates that processing conditions used in the initial simulation are correct. Therefore, the rest of the simulations concentrate on improving upon the initial process by altering processing parameters. Therefore, because the initial material characterization and processing conditions are validated, any improvements shown by the simulations are accurate.

The variation of plug temperature has no effect on the thickness distribution of the linear material model. Results of previous by Lee [23] of reverse vacuum prestretching found that sheet thickness distribution changed with mold temperature for the nonlinear material model. These results showed that small variations in sheet temperature, on the order of 20ºC, altered the thickness throughout the entire cross section. The largest alterations occurred at the corners and throughout the bottom. It is possible that the plug negates any effects of sheet temperature. It would be interesting to investigate this possibility in further studies.

Increasing draw depth changes the location along the contour of the thinnest point and increases the minimum thickness value. As a result the sheet thickness uniformity improves with increasing draw depth, resulting in fewer stress concentrations because of smaller variations in thickness. Additionally, the possibility of the sheet to develop holes decreases. Increases in draw depth also push more material to the bottom while thinning the sidewall. This shows the importance of draw depth for modifying the thermoforming operation to control the amount of thinning on the sidewall. The result matches the accepted theory of plug assist very closely [4]. The most accurate simulation to the process and lab data is the single relaxation time fluid with the deepest draw depth.

VI. Conclusion

The evidence suggests that a single time fluid should be used to characterize the polypropylene in simulations. Furthermore, altering the processing conditions to include a deeper draw depth will improve cup thickness uniformity and minimum sheet thickness. Lastly because, heat transfer between the plug and the sheet has no effect on the thickness distribution, there is no concern for unstable processing conditions due to temperature changes in the sheet or plug. Therefore, the process can be characterized as reliable and consistent.

VII. Acknowledgement

The authors are indebted to Dr. Jaydeep Kulkarni of Fluent Corporation for his technical guidance with the finite element software, and to Dr. Martin Stephenson of the Placon Corporation for his technical advice. We thank the Placon Corporation of Madison,

Wisconsin and Plastic Ingenuity, Inc. of Cross Plains, Wisconsin for their financial support through their memberships in the Industrial Consortium of the Center for Advanced Polymer and Composite Engineering at the University of Wisconsin. The Placon Corporation is also recognized for its sustaining sponsorship of the Rheology Research Center of the University of Wisconsin. Kershner is also indebted to the Society of Plastics Engineers for a scholarship awarded by the Thermoforming Division.

References

[1] Tadmor, Z. and Gogos, G.G., *Principles of Polymer Processing,* John Wiley & Sons, Inc., New York (1979).

[2] Hart-Smith, L.J. and Crisp, J.D.C., *Int. J. Eng. Sci.,* **5***,* 1(1967).

[3] Sheryshev, M.A., Zhogolev, I.V. and Salazkin, K.A., *Soviet Plast.* , **11**, 30 (1969).

[4] Williams, J.G., *J. Strain Analysis*, **5**, 49 (1970).

[5] Rosenzweig, N., Narkis, M. and Tadmor, Z., *Polymer Engineering and Science*, **19**, 946 (1979).

[6] Throne, J.L., *Plastics Process Engineering*, Marcel Dekker, New York (1979).

[7] Pearson, J.R.A., *Mechanics of Polymer Processing*, Elsevier Applied Science Publishers Ltd., London (1985).

[8] Allard, R., Charrier, J.-M., Ghosh ,A., Marangou, M., Ryan, M.E., Shrivastava, S. and Wu, R., *J. Polym. Eng.*, **6**, 363 (1986).

[9] Baird, D.G. and Collias, D.I., *Polymer Processing Principles and Design*, Butterworth-Heinemann, Boston (1995); Wiley & Sons, New York (1998).

[10] Osswald, T.A. and Hernández-Ortiz, J.P., *Polymer Processing - Modeling and Simulation*, Hanser Publishers, Munich (2006).

[11] Strong, A.B., *Plastics Materials and Processing*, 3rd ed., Prentice Hall, Upper Saddle River, New Jersey (2006).

[12] Bird, R.B., Armstrong, R.C. and Hassager, O. , *Dynamics of Polymeric Liquids, Vol. 1: Fluid Mechanics*, 2nd ed., Wiley & Sons, New York (1987); see Eq. (8.4-15).

[13] Stephenson, M.J., Dargush, G.F. and Ryan, M.E., *Polymer Engineering and Science*, **39**, 2199 (1999).

[14] Stephenson, M.J., *An Experimental and Theoretical Study of Sheet Sag in the Thermoforming Process,* PhD Thesis, State University of New York, Buffalo, NY (August 1997).

[15] Rosenzweig, N., Narkis, M., Tadmor, Z., "Wall Thickness Distribution in Thermoforming", Polymer Engineering and Science, 19, 946-951(1979)

[16] Charrier, J.-M., Shrivastava, S. "Free and Constrained Inflation of Elastic Membranes in Relation to Thermoforming-Non-Axisymetric Problems", Journal of Strain Analysis, 24, 35-72 (1979)

[17] Throne, J.L."Modelling Plug-assisted Thermoforming", Advances in Polymer Technology, 9, 309-320 (1989)

[18] Song, W.N., Mirza, F.A., Vlachopoulous, J., "Finite Element Simulation of Plug-assist Forming", International Polymer Processing, 7, 248-256 (1992)

[19] DeLorenzi, H.G., Nied, H.F., Taylor, C.A., "A Numerical/Experimental Approach to Software Development for Thermoforming Simulations", Journal of Pressure Vessel Technology, 113, 102-114 (1991)

[20] Nied, H.F., Taylor, C.A., DeLorenzi, H.G., "Three-Dimensional Finite Element Simulation of Thermoforming", Polymer Engineering and Science, 30, 1314-1322 (1990)

[21] Erchiqui, F., Gakwaya, A., Rachik, M., "Dynamic Finite Element Analysis of Nonlinear Isotropic Hyperelastic and Viscoelastic Materials for Thermoforming Applications", 45, 125-134 (2006)

[22] Erchiqui, F., Thermodynamic Approach of Inflation Process of K-BKZ Polymer Sheet With Respect to Thermoforming", Polymer Engineering and Science, 45.1319-1335 (2005)

[23] Lee, J.K., Virkler, T.L., Scott, C.E., "Effects of Rheological Properties and Processing Parameters on ABS Thermoforming", Polymer Engineering and Science, 41, 240-261 (2001)

[24] Hade, A.J., Giacomin, A. Jeffrey, "Characterization of Thermoforming Resins Using Exponential Shear", Proc. XIVth Int. Congr. On Rheology, 1-3 (2004)

[25] Osswald, T., Menges, G., "Materials science of polymers for engineers", Hanser Publishers , Munich (2003)

[26] Dealy, J., Wissbrun, K., " Melt rheology and its role in plastics processing: theory and applications", Van Nostrand Reinhold, New York (1990)